Proceedings Paper:
Latimer, I.F., Fairweather, M., Peakall, J. et al. (2023) Extended LBM-DEM and LBM-DEM-FSLBM model for gas migration through bidisperse suspensions. In: Proceeding of 10th International Symposium on Turbulence, Heat and Mass Transfer, THMT-23, Rome, Italy, 11-15 September 2023. 10th International Symposium on Turbulence, Heat and Mass Transfer, THMT-23, 11-15 Sep 2023, Rome, Italy. Begell House, Danbury, Connecticut, p. 12. ISBN: 978-1-56700-534-9. ISSN: 2377-4169. EISSN: 2377-2816.

https://doi.org/10.1615/ichmt.thmt-23.770

Turbulence, Heat and Mass Transfer 10

Extended LBM-DEM and LBM-DEM-FSLBM model for gas migration through bidisperse suspensions

I.F. Latimer[1], M. Fairweather[2], J. Peakall[3], D. Harbottle[2], M. Barnes[4], T.N. Hunter[2]

[1]*School of Computing, University of Leeds, Leeds LS2 9JT, UK, scil@leeds.ac.uk*

[2]*School of Chemical and Process Engineering, University of Leeds, Leeds LS2 9JT, UK, M.Fairweather@leeds.ac.uk, D.Harbottle@leeds.ac.uk, T.N.Hunter@leeds.ac.uk*

[3]*School of Earth and Environment, University of Leeds, Leeds LS2 9JT, UK, J.Peakall@leeds.ac.uk*

[4]*Sellafield Ltd, Hinton House, Warrington WA3 6GR, UK, martyn.g.barnes@sellafieldsites.com*

Abstract – Gas migration and retention in viscoelastic sediments is significant in many environmental and industrial settings. An extended LBM-DEM-VOF model is used to capture how gas influences sediment bed rheology based on the lattice Boltzmann modelling framework waLBerla, the discrete element method with interparticle lubrication, and the free surface LBM for liquid-gas interfaces. Modelling fluid-particle interactions is shown to be important due to the hydrodynamic forces involved in particle collisions. Fluid-particle interactions are studied using the momentum exchange method, with results showing good accuracy for different boundary condition schemes. The model is also applied to mono and bidisperse packed bed simulations to explore pressure drop. Good agreement with the Ergun equation is obtained for monodisperse beds, while well mixed bidisperse beds have a linear pressure drop and segregated beds two clearly defined regions. The ability of the lattice Boltzmann framework to capture complex fluid-particle interactions is demonstrated by the results presented.

1. Introduction

Gas growth, migration, retention and release in soft sediments is a complex and poorly understood phenomenon that holds importance within many natural and engineered settings. These range from aquatic environments, such as lakes (Keller and Stallard, 1994), rivers (Johnson et al., 2002) and shallow marine beds (Claypool and Kaplan, 1974), to industrial processes, such as hydrogen release from corroded metal cladding from nuclear activities (Allemann et al., 1991) and wastewater management (Van Kessel et al., 2002). Although a well-documented occurrence, there is a large knowledge gap regarding the fluid-structure interactions taking place in solid-liquid-gas flows. The main restricting factor for experimental investigations is sediment opacity. The majority of these particle suspensions are made up from polydisperse arrays of different opaque materials. Though finding the bulk properties of sediment samples is fairly simple, understanding the local rheological variations in different sediment mixtures is more complex. Although advanced imaging techniques, such as X-ray Computed Tomographic Imaging (CT), allow for bubble imaging within sediment beds, it is limited due to only being possible for discrete time points, usually over extended periods (Johnson et al., 2017). Though this is also due to the long retention period within these sediment samples, it means CT scan images may miss key dynamic mechanical responses of the sediment

restricting the level of understanding. Extending our knowledge of solid-liquid-gas interactions is particularly important when considering safety in industrial settings. For example, it is critical to understand the potential volume of retained hydrogen gas that may be released due to external forces during the decommissioning processes at Sellafield site (King, 2012) or whether gassy sediment beds will make a sufficiently stable environment for offshore construction due to changes in the compressibility and penetrability of the bed (Sills and Wheeler, 1992). Modern computational advances have allowed for complex fluid-particle simulations to be possible, which have the potential to accurately model dynamic interactions to a degree beyond experimental approaches.

Fluid-particle interactions is one of the most critical research areas in computational fluid dynamics. This is due to the loss of accuracy that can influence the rest of the computation, if not correctly modelled. There are two main modelling methods: Eulerian-Eulerian and Eulerian-Lagrangian (Subramaniam, 2013). Eulerian-Eulerian models capture bulk characteristics and collective behaviour of the particles well, although it cannot predict individual particle behaviour and interactions. On the other hand, Eulerian-Lagrangian models can easily obtain detailed fluid-particle and particle-particle interactions. Some papers even claim that Eulerian-Eulerian approaches incur a loss of accuracy, such as in Vegendla et al. (2011) where Eulerian-Eulerian approaches were shown to differ from experimental results, whilst the Eulerian-Lagrangian model was consistently accurate. The lattice Boltzmann method (LBM) coupled with the discrete element method (DEM), which we use in this research, is an example of a Eulerian-Lagrangian approach. Although this approach has the advantage of modelling individual particle interactions, the computational expense is much greater than in Eulerian-Eulerian method for the same scale and number of particles simulated.

In this work, the numerical approach is used to explore the relationships between solid-fluid and fluid-gas interactions, ultimately to combine them to simulate solid-fluid-gas interactions within the context of gas migration and retention in sediment beds. LBM is used and applied using the multi-physics framework waLBerla (Erlangen, Germany) (Godenschwager et al., 2013; Bauer et al., 2021). Validation and calibration studies are conducted to develop accurate simulations for mono- and bidisperse beds. This is then applied to analyzing the effect of particle segregation on the pressure drop in bidisperse beds. We focus on understanding microscale interactions in small domains as it is currently impossible to simulate industrial scale domains using this method due to high computational costs. However, the aim is to extend this research from single bubble interactions to polydisperse bubble populations. Currently, the closest LBM-DEM model for gas-liquid-solid interactions within this context is by Wang et al. (2020). The paper also briefly touches upon a model for bubble interactions with cohesive sediments, although this is restricted to two dimensional cases due to coupling complexity and computational cost. All other cases explored in this paper are three dimensional, though currently restricted to solid-fluid and fluid-gas simulations.

2. Numerical Method

Solid-fluid interactions were simulated using a four-way coupled LBM-DEM algorithm originally developed for fluidized beds by Rettinger and Rude (2018), which uses the momentum exchange method (MEM) to model the fluid and particulate phases. Particle interactions are accounted for using DEM with linear contact forces. Fluid-gas interactions were implemented using the free surface lattice Boltzmann method (FSLBM). The FSLBM uses lattice cells to represent regions of liquid, gas and their interface. The simulation is simplified by reducing the system from a two-phase flow to a single-phase flow using a volume of fluid

(VOF) approach. This simplification means that computations are neglected in gas filled cells, with a focus on the boundary treatment between the connecting interfaces. The pressure due to gas volume and surface tension is also accounted for. The main restriction to this method is that the pressure flux within the bubble is not explicitly determined.

2.1 The lattice Boltzmann method

Unlike traditional computational fluid dynamic methods that rely on macroscopic variables such as velocity and pressure for solving the Navier-Stokes equations, the lattice Boltzmann approach solves the kinetic equations for particle distribution functions (PDFs) (Succi, 2001). The macroscopic quantities (such as mass density and momentum density) can be obtained by evaluating the hydrodynamic moments of the PDFs (Krüger et al., 2017).

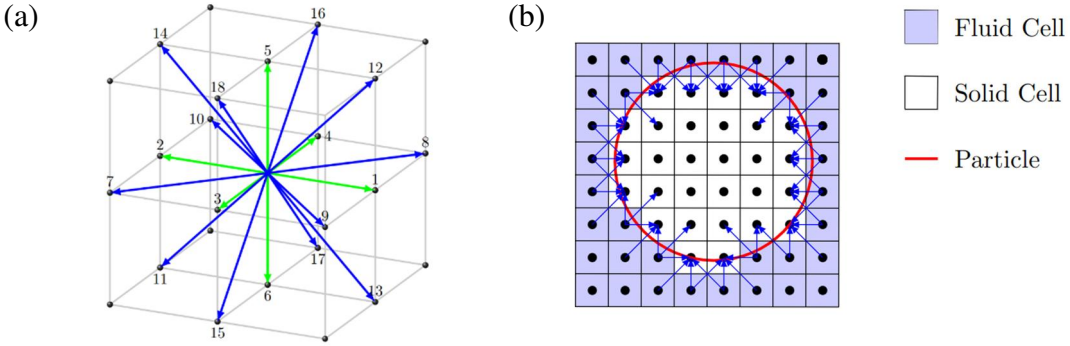

Figure 1: (a) D3Q19 lattice cell schematic (D is the number of dimensions, Q the number of PDFs), and (b) a visual representation of the moment-exchange method explicit particle mapping. Fluid-solid interaction directions are represented by blue arrows for a randomly placed particle in a uniform Cartesian lattice grid.

The computational domain is discretized into Cartesian cells each represented by a lattice. Simulations in this paper use the D3Q19 lattice, as shown in Fig. 1, unless stated otherwise. For this lattice, the PDFs are given by f_q where $q \in \{0,\ldots,18\}$ and are associated with a lattice velocity, c_q. The lattice Boltzmann equation is given by a collision step and a streaming step. The general equation for the collision step is given as follows (Krüger et al., 2017):

$$\tilde{f}_q(\boldsymbol{x},t) = f_q(\boldsymbol{x},t) + \mathcal{C}_q(\boldsymbol{x},t) + \mathcal{F}_q(\boldsymbol{x},t), \tag{1}$$

where $\mathcal{C}_q$ is the collision operator and $\mathcal{F}_q$ the external forcing operator. The streaming step is given by:

$$f_q\left(\boldsymbol{x} + c_q\Delta t, t + \Delta t\right) = \tilde{f}_q(\boldsymbol{x},t), \tag{2}$$

where the post collision operator from Eq. (1) is distributed to the corresponding neighbour lattice cells. Macroscopic quantities are calculated by taking the moments of the PDFs.

2.2 Momentum exchange method

MEM for solid-fluid interactions works by explicitly mapping the particle into the fluid domain, marking the contained cells as ‘solid’ and applying appropriate boundary conditions. All cells within this particle boundary are considered solid. A visual representation is shown in Fig. 1.

The hydrodynamic force $\boldsymbol{F}_{p,i}^{f_q}$ and the torque force $\boldsymbol{T}_{p,i}^{f_q}$ acting on the particle i are computed using the link-based momentum exchange concept.

One of the main conditions for particle modelling is that the macroscopic flow velocity must match the particle's velocity on the surface boundary. MEM achieves this by enforcing a no-slip boundary condition between the fluid and solid cells. There are multiple ways to enforce this condition, the simplest being the bounce back scheme (BB) (Ladd, 1994). Other common schemes include central linear interpolation (CLI) and multi-reflection (MR).

The BB scheme is given by:

$$f_{\bar{q}}(\boldsymbol{x}, t + \Delta t) = \tilde{f}_q(\boldsymbol{x}, t) - 2\frac{\omega_q}{c_s^2}\rho_0 \boldsymbol{v}(\boldsymbol{x}_b, t).\boldsymbol{c}_q, \tag{3}$$

where $\boldsymbol{v}$ is the velocity at the boundary position $\boldsymbol{x}_b$, located mid-way between the fluid cell and solid cell centers. The velocity is obtained from the formula:

$$\boldsymbol{v}(\boldsymbol{x}, t) = \boldsymbol{U}_p(t) + \Omega_P(T) \times (\boldsymbol{x} - \boldsymbol{X}_p(t)), \tag{4}$$

where $\boldsymbol{U}_p$ is the particle's transitional velocity, Ω_p is the rotational velocity and $\boldsymbol{X}_p$ is the centre of mass of the particle. The BB scheme is the least advanced of the MEM boundary methods. When the shape, size and hence boundary location of the particle are known, more complex (and accurate) boundary schemes can be applied such as the CLI and MR schemes.

Lubrication correction was incorporated into the original code (Rettinger and Rude, 2018) by use of a fluid-solid interaction force model. This force term comes into effect to account for the lubrication forces between two solid surfaces when the gap between them becomes too small to accurately compute. The force $\boldsymbol{F}^{q_{f\to s}}$, acting on a solid boundary $\boldsymbol{x}_b$, over the fluid to solid link (denoted $q_{f\to s}$), can be calculated using:

$$F^{q_{f\to s}}(\boldsymbol{x}_b, t) = \frac{(\Delta x)^3}{\Delta t}\left[\left(c_{q_{f\to s}} - \boldsymbol{v}(\boldsymbol{x}_b, t)\right)\tilde{f}_{q_{f\to s}}(\boldsymbol{x}, t) - (\boldsymbol{c}_{\bar{q}_{f\to\to s}} - \boldsymbol{v}(\boldsymbol{x}_b, t)) f_{\bar{q}_{f\to s}}(\boldsymbol{x}, t + \Delta t)\right]. \tag{5}$$

The MEM is used here and describes the force as the difference between the momentum towards the boundary and that away from the boundary. Summing up the local contributions, the total hydrodynamic forces and torques acting on the solid particle can be obtained. The last step is to update all the cells to their new solid or fluid status and reconstruct the PDF information as appropriate. Missing PDFs are obtained by extrapolating the neighbouring fluid cell PDFs in a normal direction.

2.3 Free surface lattice Boltzmann method

The FSLBM reduces the two-phase flow problem to single-phase with a free boundary, under the assumption that the dynamics of the gas phase can be neglected. A single-phase LBM (governed by the collision and streaming steps for the generalized Navier-Stokes equations, as given in Eqs. (1) and (2)) is used to simulate the liquid phase. For the fluid-gas boundary, a VoF approach is used. In these simulations, cells are defined either as fluid, gas or interface. Interface lattice cells form a close layer between the liquid and gas cells. The volume (or mass flux) of these interface cells is tracked and has a fill level, φ, between one and zero. A fill level

of zero indicates an empty cell (i.e. gas) and a fill level of one indicates a filled lattice (completely liquid). The mass for each cell can be computed using:

$$m = \varphi(\Delta x^3)\rho, \tag{6}$$

where ρ is the local density.

For the interface cells, the mass exchange is calculated using the stream step of the LBM and corresponds to the change in the value φ. An interface cell at x will have mass balance with a neighbour $x + c_\alpha$ given by:

$$\Delta m_\alpha = \begin{cases} 0 & \text{if } \boldsymbol{x} + \boldsymbol{c}_\alpha \text{ is gas,} \\ f_{\bar{\alpha}}(\boldsymbol{x} + \boldsymbol{c}_\alpha, t) - f_\alpha(\boldsymbol{x}, t) & \text{if } \boldsymbol{x} + \boldsymbol{c}_\alpha \text{ is liquid,} \\ \frac{1}{2}\left(\varphi(\boldsymbol{x}, t) + \varphi(\boldsymbol{x} + \boldsymbol{c}_\alpha, t)\right) \cdot \left(f_{\bar{\alpha}}(\boldsymbol{x} + \boldsymbol{c}_\alpha, t) - f_\alpha(\boldsymbol{x}, t)\right) & \text{if } \boldsymbol{x} + \boldsymbol{c}_\alpha \text{ is interface.} \end{cases} \tag{7}$$

No computation takes place for the gas cells, and hence they have no lattice and the interface cells have missing PDFs after the streaming step. The missing PDFs are reconstructed as in Anderl et al. (2014) only towards the free surface using:

$$f_\alpha^{\text{liquid}}(\boldsymbol{x}, t) = f_\alpha^{\text{gas}}(\boldsymbol{x}, t) + f_{\bar{\alpha}}^{\text{gas}}(\boldsymbol{x}, t) - f_{\bar{\alpha}}^{\text{liquid}}(\boldsymbol{x}, t). \tag{8}$$

The gas pressure is given by:

$$p_{\text{gas}} = p_v + \Delta p_\sigma, \tag{9}$$

where p_v denotes the bubble pressure and Δp_σ denotes the Laplace pressure, with:

$$p_v = \frac{\text{initial bubble volume}}{\text{current bubble volume}} \cdot p_0, \tag{10}$$

where the initial pressure can be written as $P_0 = \rho_0 c_s^2$ and ρ_0 is trivially taken to be 1. The Laplace pressure required for capturing the effects due to surface tension can be computed as:

$$\Delta p_\sigma = 2\sigma\kappa(x, t), \tag{11}$$

where σ is the surface tension constant and κ is the local curvature.

A bubble model is used to track unconnected gas regions as distinct bubbles with their own individual pressures. Each bubble is represented by a data set containing important data for modelling (e.g. current and initial volume required for calculating pressure in Eq. (10)) denoted by a unique bubble ID, updated each timestep. This is simple for bubbles which do not interact, however, it is more complicated for splitting or coalescing bubbles. The FSLBM module in waLBerla utilizes a flood fill algorithm which extracts the connectivity data and updates the bubble IDs. This algorithm is only used when the connectivity between the gas phase changes (i.e. when the number of discrete bubbles varies due to coalescence or splitting).

2.4 Bidisperse bed setup

For the bidisperse bed simulation using spherical particles of 200 and 800 μm diameter, a

rectangular domain is discretized into [20 × 20 × 200] cells representing a 2mm × 2mm × 10mm domain. Inflow is set at the top boundary, with outflow at the bottom with a particle-only restriction, to prevent particles from leaving the domain. Periodic boundary conditions are used for the remaining planes. Particles are created randomly and allowed to fall under gravity, creating a mixed bed which is subsequently resolved via DEM-only steps to account for any particle overlaps caused during packing. After the bed has been created, a constant laminar fluid flow is started. Bed segregation is caused through the downwards fluid flow and particle interaction with the bottom plane. Particle position, density and pressure are recorded over time.

3. Results and Discussion

Below we discuss the initial validation studies for two phase solid-liquid and liquid-gas flows undertaken in building towards a three-phase model for bubble migration in sediment beds.

3.1 Lubrication correction

For suspensions containing high volume fractions, surface-surface collisions are bound to occur. These collisions play a crucial role in contributing to the momentum balance of the suspension, and therefore modelling them accurately is essential. As with any computational approach, the discretization of the domain is a major factor which influences accurate modelling, with a need to balance accuracy with computational expense, especially when modelling large numbers of small particles in a reasonably sized domain. In the case of a particle-particle collision, a thin layer of liquid forms between the two surfaces. As the gap size decreases, this fluid is squeezed out then pushed back into the gap as the particles rebound. Due to this, the hydrodynamic forces increase. Unfortunately, numerical simulations fail to capture this effect, hence an explicit correction term is required (Nguyen and Ladd, 2002).

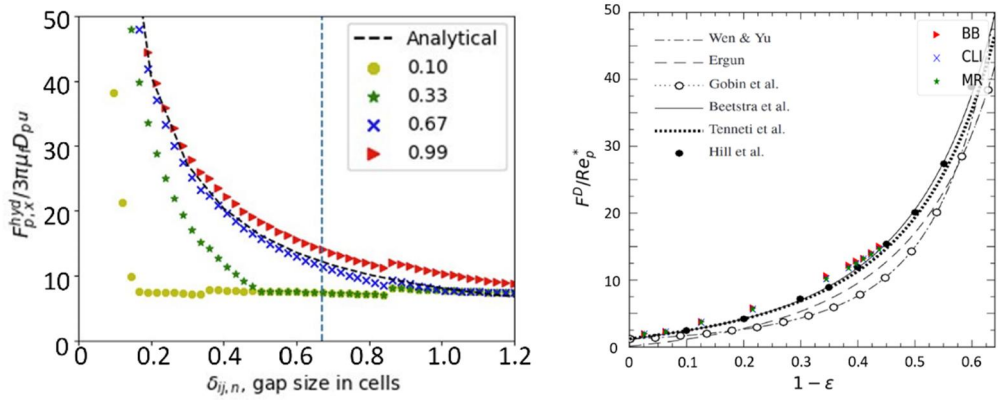

(a) (b)

Figure 2: (a) Hydrodynamic force on sphere as a function of gap size for case of equally sized sphere-sphere collisions. Lubrication correction applied once gap between colliding spheres reaches a certain distance (here 0.10, 0.33, 0.67 and 0.99) where the cell size is 1. Simulation results compared to an analytical equation for hydrodynamic force between two colliding spheres (Ding and Aidun, 2003). (b) LBM simulation results using MEM for different boundary conditions (BB, CLI, MR) compared to data in Simonin et al. (2016), models in literature (Ergun, 1952; Wen, 1966; Gobin et al., 2003; Beestra et al., 2007), IBM data (Tenneti et al., 2011) and LBM data (Beestra et al., 2007; Hill et al., 2001).

As previously mentioned, the lubrication forcing term is only used when the gap between two colliding surfaces becomes too small. The aim of this study was to determine the

appropriate cut-off distance for using the lubrication forcing term related to lattice cell size. To achieve this, a two-particle normal collision was created with the lubrication forcing term applied for the cut off distances $\delta_{ij} = 0.1, 0.33, 0.67$ and 0.99, where δ_{ij} is the gap size in cells.

Results can be seen in Fig. 2 and clearly show how the choice of lubrication cut-off distance can significantly impact the short-range hydrodynamic force interactions. Evidently, δ_{ij}=0.67 is the ideal lubrication cut-off distance, since smaller δ_{ij} choices significantly under-estimate the hydrodynamic forces. Although the cut off distances δ_{ij}=0.99 is reasonably accurate upon impact, it over-estimates the hydrodynamic force in regions. Additionally, choosing the smallest cut-off distance possible reduces the amount of computation required.

3.2. Drag force on mono-sphere arrays

Here, computation of the fluid-solid interaction force is evaluated for Stokes flow past an infinite array of equally spaced monodisperse spheres. The simulation is run until convergence, and is used to compare the different MEM boundary conditions, namely BB, CLI and MR. Results of the simulation are plot for the dimensionless drag force against the solid volume fraction in Fig. 2.

Results are in good agreement for all boundary conditions. Figure 2 shows particularly good agreement between the Tenneti drag force correlation, which we will implement in later developments of the code. The CLI and MR simulations took marginally longer times to run for negligible increase in modelling accuracy, therefore the decision is currently to continue modelling with the BB boundary condition. However, it should be noted that this is an extremely simple model, and therefore boundary conditions may need to be re-evaluated later on when modelling more complex flows.

3.3. Pressure drop over randomly packed sphere beds

Randomly packed monodisperse sediment beds of around 50 spheres were generated to observe if we can sustain the accuracy obtained from the static array of equally spaced spheres. Once again, spheres were fixed in space, however, to create the random packing, they were allowed to fall into the domain under gravity. No-slip boundary conditions were applied to the sphere surfaces, and a constant flow was driven from the bottom to the top of the bed. The pressure drop was computed and void fraction calculated, with four test cases of similar void fractions compared. Simulation results and the corresponding non-dimensional pressure drops can be found in Tables 1 and 2 respectively.

Table 1: Simulation results for four randomly packed bed test cases. Particle diameter D_p = 500 μm for Cases 1-2, D_p = 1000 μm for Cases 3-4. Note that values are given in their LB units.

Test case	Pressure drop	Average velocity	No. fluid cells	No. solid particles	Void fraction
1	6.3×10^{-3}	6.0×10^{-3}	9099477	51	0.56
2	5.9×10^{-3}	6.5×10^{-3}	9067491	52	0.58
3	6.3×10^{-3}	6.4×10^{-3}	9099446	51	0.54
4	5.7×10^{-3}	6.4×10^{-3}	9163522	49	0.58

The non-dimensional pressure drop across the bed was calculated using the Ergun equation (Ergun, 1952), as given by:

$$\frac{\Delta P}{H} = \frac{150\mu\bar{u}(1-\varepsilon)^2}{D_p^2\varepsilon^2} + \frac{1.75\rho\bar{u}^2(1-\varepsilon)}{D_p\varepsilon^3}. \quad (12)$$

Note that the lattice pressure drop is not the same as the non-dimensional pressure drop, in the same way the non-dimensional pressure drop is not the actual pressure drop across the bed.

In general, the relative errors between the Ergun predicted pressure drop and the LBM simulated value are fairly small. Only Case 3 stands out as being significantly different to the others, with a 19% error.

Table 2: Non-dimensional pressure drop values and corresponding errors. Note that the non-dimensional pressure drop is not the same as the LB pressure drop.

Test case	Non-dimensional pressure drop		Relative error (%)
	LBM	Ergun	
1	6.38	6.23	2
2	5.93	5.47	8
3	6.33	7.81	19
4	5.72	5.51	3

The packing for Case 3 was much more structured (with almost in-line layers) unlike the random packing that was visible in Cases 1, 2 and 4. This difference in packing can be observed in Fig. 3 (where Cases 1 and 3 are compared). There was also a distinct difference in the flow characteristics moving through each bed. The flow exiting the Case 1 bed was much more chaotic than from Case 3, which appeared almost immediately laminar. This difference in packing structures potentially explains why there is an under-prediction from the simulation in comparison to experiment using Eq. (12). It is possible that simply increasing the number of particles involved would reduce this error. However, it should also be noted that this was quite a computationally expensive simulation considering how small the bed volume considered was.

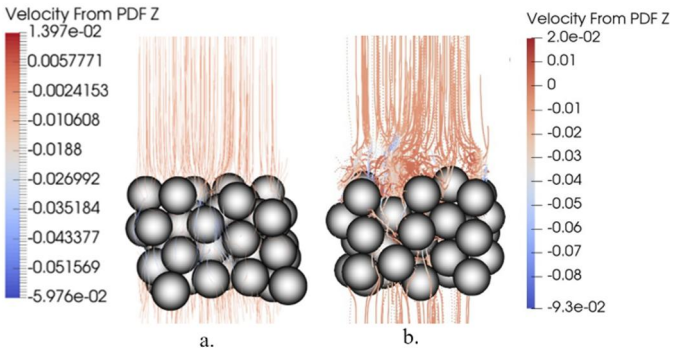

Figure 3: Streamlines through different random packings for (a) Case 3 and (b) Case 1.

3.4. Pressure drop due to bed segregation

To create a bed model capable of capturing the mechanical responses of the sediment from the forces exerted by a trapped or migrating gas bubble, an unconsolidated bed is required. For the context of this paper, unconsolidated refers to the particles not being fixed, but rather malleable to the flow and external forces. Unlike in earlier sections, larger sphere beds are used, with the number of particles approximately $\mathcal{O}(10^6)$. In this section, we consider results for a bidisperse system with an equal distribution of 200 and 800 μm diameter spheres. These values were

chosen as an extreme case where segregation can be forced relatively quickly.

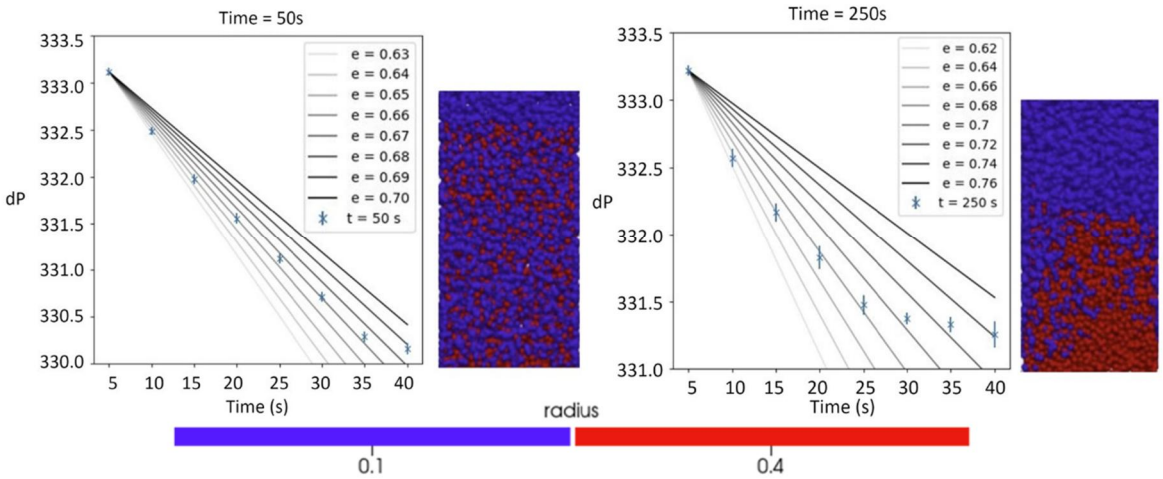

Figure 4: Pressure drop in a bidisperse bed of 200 μm (blue) and 800 μm (red) diameter spheres undergoing forced segregation for times (a) t = 50 s and (b) t = 250 s. The straight lines (grey) show the predicted pressure drop for different void ratios using the Ergun equation (Eq. (12)).

A linear pressure drop is predicted for these regimes according to the Ergun equation. Since the void fraction is changing in these simulations, we have plotted the predictions for a range of void fractions, given by the straight lines in Fig. 4. The average mass diameter of the particle is used. Although not shown, earlier results for monodisperse sphere beds under the same set-up showed good agreement when compared to the Ergun equation for both fixed and cohesive spheres. When segregation was enforced, two distinct linear regions of pressure change can be seen as expected. For well mixed particle beds, using the average mass diameter in the Ergun equation gives a reasonably accurate prediction for the pressure drop across the bed. However, for the segregated bed, the pressure drop can be split into two regions corresponding to the different sphere diameters. Some of the simulated void ratios in different regions appear larger than expected (Mauret and Renaud, 1997), although this is likely to be a consequence of forcing segregation in small beds over short time periods. Future work will look to increase the number of particles and height of the bed to see if this produces more physically validated voidages. Nonetheless, since by forcing segregation, we are creating a slight fluidization of the bed which may also account for the larger void ratios (though it is important to note that the flow rate is chosen so that the bed reaches a maximum swell and no individual particles leave the bed).

3.4. Rising bubble shape

These simulations consider the shape and FSLBM capability for meshing and modelling the behaviour of a single gas bubble rising in a stagnant Newtonian fluid. The bubble properties are determined by the Evötös number ($\Delta\rho\ g\ L^2/\gamma$, where $\Delta\rho$ is the difference in density of the two phases, g gravitational acceleration, L^2 a characteristic length relating to curvature of the bubble and γ is the surface tension), which considers the influence of the gravitational forces compared to surface tension, and the Morton number ($g\mu_c^4\Delta\rho/\rho_c^2\sigma^3$, where g is gravitational acceleration, μ_c the viscosity of the surrounding fluid, ρ_c the density of the surrounding fluid and σ is the surface tension coefficient) that (with the Evötös number) determines the shape of the bubble moving within the fluid (Aybers and Tapucu, 1969; Duineveld, 1995). The FSLBM module simulations are validated against experimental results from Legendre et al. (2012) on bubbles rising in Newtonian fluids with different material properties (see Table 3).

Table 3: Fluid properties for rising bubble experiments for water-glycerin ('W-G') mixtures (from Legendre et al. (2012)).

Fluid W-G ratio	Density (kg m^{-3})	Viscosity (mPa s)	Surface tension (mN m^{-1})	Morton Number
100/0 W-G	1000	1.0	72.5	2.5×10^{-11}
25/75 W-G	1191	19.9	65.7	4.6×10^{-6}
11/89 W-G	1225	80.0	62.7	1.3×10^{-3}
8/92 W-G	1242	173.5	62.6	2.9×10^{-2}
4/96 W-G	1258	457.8	58.8	1.7×10^{0}

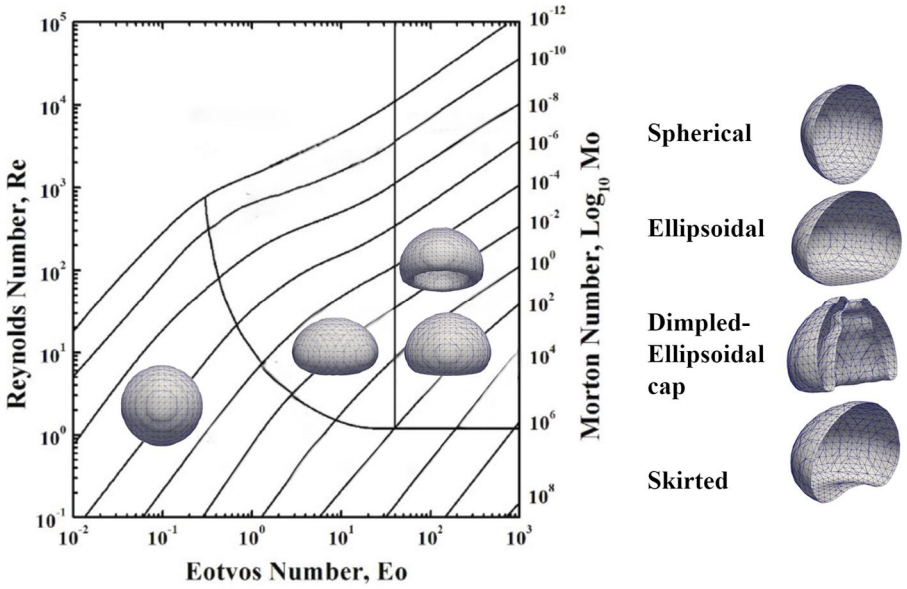

Figure 5: Bubble mesh shape using FSLBM in Newtonian fluid under different fluid mediums as detailed in Table 3. Bubble meshes are compared to predicted shapes from Legendre et al. (2012).

Results for a single bubble rising in a Newtonian fluid can be found in Fig. 5. They show extremely good agreement with experimental observations in Legendre et al. (2012) and predicted shape regimes detailed in Clift et al. (2005). There is currently on-going work to extend this to non-Newtonian fluids, and to incorporate particle beds in three phase simulations to understand how anisotropy affects the bubble shape and migration behaviour.

9. Conclusions

This paper presented initial development and validation studies for packed bed simulations using the lattice Boltzmann framework waLBerla. The importance of incorporating lubrication correction into dense particle models was demonstrated by a two-particle collision and then subsequently included in the more advanced models. Investigations into different boundary conditions for the momentum exchange method concluded that the bounce back method was as accurate as other more intricate approaches but computationally less expensive. This conclusion may need to be revised for larger, more complex beds. Pressure drop simulations showed accurate results against the Ergun equation for all modelled beds, with bidisperse bed simulations show promising results for how segregation effects the pressure drop in particle beds. Two distinct regions were seen in the pressure drop once full segregation had been

reached. Although the difference in pressure drop was relatively small between the mixed and segregated beds, once scaled to larger beds, these results could become more significant. Further work is required to explore how bed segregation and pressure drop link to bed voidage, and to consider more poly-disperse cases. Initial validation studies using waLBerla's FSLBM module show accurate results for modelling gas shape and migration in Newtonian fluids. These simulations will be extended to non-Newtonian cases and three phase solid-liquid-gas flows.

So far, waLBerla has been shown to be a suitable LBM framework for multiphase modelling of fluid-gas and fluid-solid interactions. Work is ongoing to develop a novel coupling for liquid-solid-gas interactions to explore gas migration and retention within sediment beds. Once achieved, such multiscale modelling methods are attractive for industrial applications, however more work is required regarding physical modelling and numerical implementation before they are suitable for industry standards and implementation. In particular, an extremely powerful parallelizable capability is required to achieve large multiscale simulations.

9. Acknowledgements

The authors thank the Engineering and Physical Sciences Research Council, UK and Sellafield Ltd. for funding through the Centre for Doctoral Training in Fluid Dynamics (EP/S022732/1).

References

1. M. Keller and R.F. Stallard. Methane emission by bubbling from Gatun Lake, Panama. *J. Geophys: Atmospheres.*, 99: 8307-8319, 1994.
2. B.D. Johnson, B.P. Boudreau, B.S. Gardiner and R. Maass. Mechanical response of sediments to bubble growth. *Mar. Geol.*, 187: 347-363, 2002.
3. G.E. Claypool and I.R. Kaplan. The origin and distribution of methane in marine sediments. *Natural gases in marine sediments*. Springer, 1974.
4. R.T. Allemann, Z.I. Antoniak, J.R. Friley, C.E. Haines, L.M. Liljegren and S. Somasundaram. Collection and analysis of existing data for waste tank mechanistic analysis. *Tech. Rep. Pacific Northwest Lab.*, Richland, WA (United States), 1991.
5. T. Van Kessel and W.G.M. Van Kesteren. Gas production and transport in artificial sludge depots. *J. Waste Manag.*, 22: 19-28, 2002.
6. M.C. Johnson, M. Fairweather, D. Harbottle, T.N. Hunter, J. Peakall and S.R. Biggs. Yield stress dependency on the evolution of bubble populations generated in consolidated soft sediments. *AIChE J.*, 63: 3728-3742, 2017.
7. F. King. Gaseous hydrogen issues in nuclear waste disposal. In *Gaseous Hydrogen Embrittlement of Materials in Energy Technologies*. Elsevier, 2012.
8. G.C. Sills and S.J. Wheeler. The significance of gas for offshore operations. *Cont. Shelf Res.*, 12: 1239-1250, 1992.
9. S. Subramaniam. Lagrangian-Eulerian methods for multiphase flows. *Prog. Energy Combust. Sci.*, 39: 215-245, 2013.
10. S P. Vegendla, G.J. Heynderickx and G.B. Marin, Comparison of Eulerian-Lagrangian and Eulerian-Eulerian method for dilute gas–solid flow with side inlet. *Comput. Chem. Eng.*, 35: 1192-1199, 2011.
11. C. Godenschwager, F. Schornbaum, M. Bauer, H. Köstler and U. Rüde. A framework for hybrid parallel flow simulations with a trillion cells in complex geometries. *Int. Conf. High Perform. Comput.*, 2013.
12. M. Bauer, S. Eibl, C. Godenschwager, N. Kohl, M. Kuron, C. Rettinger, F. Schornbaum, C. Schwarzmeier, D. Thönnes, H. Köstler and U. Rüde. waLBerla: A block-structured

high-performance framework for multiphysics simulations. *Comput. Math. with Appl.*, 81: 478-501, 2021.
13. M. Wang, Y.T. Feng, Y. Wang, T.M. Qu and W. He. A hybrid discrete bubble-lattice Boltzmann-discrete element model for gas-charged sediments. *Comput. Part. Mech.*, 7: 509-522, 2020.
14. C. Rettinger and U. Rüde. A coupled lattice Boltzmann method and discrete element method for discrete particle simulations of particulate flows. *Comput. Fluids*, 172: 706-719, 2018.
15. S. Succi. *The lattice Boltzmann equation: For fluid dynamics and beyond*. Oxford University Press, 2001.
16. T. Krüger, H. Kusumaatmaja, A. Kuzmin, 0. Shardt, G. Silva and E.M. Viggen. The lattice Boltzmann method. *Springer International Publishing*, 2017.
17. A.J.C. Ladd, Numerical simulations of particulate suspensions via a discretized Boltzmann equation. Part 1. Theoretical foundation. *J. Fluid Mech*, 271: 285-309, 1994.
18. D. Anderl, S. Bogner, C. Rauh, U. Rüde and A. Delgado, Free surface lattice Boltzmann with enhanced bubble model. *Comput. Math. with Appl.*, 67: 331-339, 2014.
19. N.Q. Nguyen and A.J.C. Ladd, Lubrication corrections for lattice-Boltzmann simulations of particle suspensions. *Phys. Rev. E.*, 66: 046708, 2002.
20. E.J. Ding and C.K. Aidun, Extension of the lattice-Boltzmann method for direct simulation of suspended particles near contact. *J. Stat. Phys.*, 112: 685-708, 2003.
21. O. Simonin, S. Chevrier, F. Audard and P. Fede, Drag force modelling in dilute to dense particle-laden flows with mono-disperse or binary mixture of solid particles. *Int. Conf. Multiph. Flow*., 2016.
22. S. Ergun, Fluid flow through packed columns. *Chem. Eng. Prog.*, 48: 89-94, 1952.
23. C.Y. Wen, Mechanics of fluidization. *Fluid Particle Technology, Chem. Eng. Progress. Symposium Series*, 62: 100-111, 1966.
24. A. Gobin, H. Neau, O. Simonin, J.R. Llinas, V. Reiling and J.L. S´elo, Fluid dynamic numerical simulation of a gas phase polymerization reactor. *Int. J. Numer. Fluids*. 43: 10-11, 2003.
25. R. Beetstra, M.A. van der Hoef and J.A.M. Kuipers. Drag force of intermediate Reynolds number flow past mono-and bidisperse arrays of spheres. *AIChE J.*, 53: 489-501, 2007.
26. S. Tenneti, R. Garg and S. Subramaniam. Drag law for monodisperse gas-solid systems using particle-resolved direct numerical simulation of flow past fixed assemblies of spheres. *Int. J. Multiph. Flow*., 37: 1072-1092, 2011.
27. R.J. Hill, D.L. Koch and A.J.C. Ladd. The first effects of fluid inertia on flows in ordered and random arrays of spheres. *J. Fluid. Mech*., 448: 213-241, 2001.
28. E. Mauret and M. Renaud. Transport phenomena in multi-particle systems – I. Limits of applicability of capillary model in high voidage beds-application to fixed beds of fibers and fluidized beds of spheres, *Chem. Eng. Sci.*, 52: 1807-1817, 1997.
29. N.M. Aybers and A. Tapucu. Studies on the drag and shape of gas bubbles rising through a stagnant liquid. *Heat Mass Transf.*, 2: 171-177, 1969.
30. P.C. Duineveld. The rise velocity and shape of bubbles in pure water at high Reynolds number. *J. Fluid Mech.*, 292: 325-332, 1995.
31. D. Legendre, R. Zenit and J.R. Velez-Cordero, On the deformation of gas bubbles in liquids. *Phys. Fluids.*, 24: 043303, 2012.
32. R. Clift, J.R. Grace and M.E. Weber. *Bubbles, Drops, and Particles*. Dover Publications, 2005.